Real time 4D IMRT treatment planning based on a dynamic virtual patient model: Proof of concept

Bingqi Guo[a)]
Radiation Oncology, University of Michigan, Ann Arbor, Michigan 48109

X. George Xu
Nuclear Engineering and Engineering Physics, Rensselaer Polytechnic Institute, Troy, New York 12180

Chengyu Shi
Radiation Oncology, St. Vincent's Medical Center, Bridgetport, Connecticut 06606

(Received 16 November 2010; revised 28 March 2011; accepted for publication 28 March 2011; published 6 May 2011)

Purpose: To develop a novel four-dimensional (4D) intensity modulated radiation therapy (IMRT) treatment planning methodology based on dynamic virtual patient models.
Methods: The 4D model-based planning (4DMP) is a predictive tracking method which consists of two main steps: (1) predicting the 3D deformable motion of the target and critical structures as a function of time during treatment delivery; (2) adjusting the delivery beam apertures formed by the dynamic multi-leaf collimators (DMLC) to account for the motion. The key feature of 4DMP is the application of a dynamic virtual patient model in motion prediction, treatment beam adjustment, and dose calculation. A lung case was chosen to demonstrate the feasibility of the 4DMP. For the lung case, a dynamic virtual patient model (4D model) was first developed based on the patient's 4DCT images. The 4D model was capable of simulating respiratory motion of different patterns. A model-based registration method was then applied to convert the 4D model into a set of deformation maps and 4DCT images for dosimetric purposes. Based on the 4D model, 4DMP treatment plans with different respiratory motion scenarios were developed. The quality of 4DMP plans was then compared with two other commonly used 4D planning methods: maximum intensity projection (MIP) and planning on individual phases (IP).
Results: Under regular periodic motion, 4DMP offered similar target coverage as MIP with much better normal tissue sparing. At breathing amplitude of 2 cm, the lung V_{20} was 23.9% for a MIP plan and 16.7% for a 4DMP plan. The plan quality was comparable between 4DMP and IP: PTV V_{97} was 93.8% for the IP plan and 93.6% for the 4DMP plan. Lung V_{20} of the 4DMP plan was 2.1% lower than that of the IP plan and D_{max} to cord was 2.2 Gy higher. Under a real time irregular breathing pattern, 4DMP had the best plan quality. PTV V_{97} was 90.4% for a MIP plan, 88.6% for an IP plan and 94.1% for a 4DMP plan. Lung V_{20} was 20.1% for the MIP plan, 17.8% for the IP plan and 17.5% for the 4DMP plan. The deliverability of the real time 4DMP plan was proved by calculating the maximum leaf speed of the DMLC.
Conclusions: The 4D model-based planning, which applies dynamic virtual patient models in IMRT treatment planning, can account for the real time deformable motion of the tumor under different breathing conditions. Under regular motion, the quality of 4DMP plans was comparable with IP and superior to MIP. Under realistic motion in which breathing amplitude and period change, 4DMP gave the best plan quality of the three 4D treatment planning techniques. [DOI: 10.1118/1.3578927]

Key words: 4D IMRT, virtual patient models, treatment planning, respiratory motion

I. INTRODUCTION

Respiratory motion causes dose errors in radiation therapy treatment planning and delivery.[1] For intensity modulated radiation therapy (IMRT), tracking using the dynamic multi-leaf collimators (DMLC) is one of the most efficient methods of motion management. The tracking method measures the motion of the tumor and adapts the DMLCs to follow the tumor motion.[2] To compensate for rigid target motion, theoretical methods have been proposed to superimpose one dimensional (1D),[3,4] two dimensional (2D),[4–6] and three dimensional (3D)[7–10] target trajectories onto MLC leaf trajectories.[11] To compensate for deformable target motion, four dimensional computed tomography (4DCT) is commonly used. Three-dimensional IMRT plans were individually developed on all phases of the 4DCT and 4D leaf sequencing algorithms were then used to combine the plans on individual phases.[12] Though using different algorithms to account for motion, these "conventional" tracking methods have the same workflow: measuring the target motion prior to treatments, creating 4D leaf sequences in treatment planning to account for motion, and delivering the 4D leaf

sequences in treatments. Accurate tracking requires the motion of the tumor during treatment delivery to be consistent with the motion measured prior to treatment. However, studies have shown that significant changes in tumor motion exist from one delivery fraction to another[13] or even within a fraction.[14,15] Therefore, to account for the realistic motion of the tumor during an IMRT delivery fraction, real time tracking methods have been investigated. Similar to "conventional" tracking, real-time tracking first acquires prior information of the tumor motion and then creates the 4D leaf sequences. During a realistic delivery, the real-time tumor motion was measured and the leaf sequences for a 4D delivery were then modified online to account for the difference between measured and planned motions. Prediction methods[1,16–18] were usually used in real time tracking to account for the latency effect between the detection of motion to the modification of the delivery beam. The Synchrony system (Accuray, Sunnyvale, CA) is an example of real-time tracking delivery. Synchrony measures the target motion using a combination of infrared cameras and x-ray and accounts for the motion using a robotic arm.[19] For IMRT, Sawant *et al.*[20] proposed a real time tracking method for 3D rigid target motion and proved that the geometric accuracy of this method was less than 2 mm for respiratory motion.[21] However, both synchrony and Sawant's method did not consider the deformation of the targets. Yi *et al.*[22] took another approach for real time tracking: the programmed 4D leaf sequences were delivered with dose rate regulated online to account for the change of breathing pattern during treatment deliveries. This method only considered the change of breathing frequency, although the change of breathing amplitude may also affect the tracking accuracy. Another common problem of current real time tracking methods is that these methods do not consider the interplay effect of the motion of tumor and the motion of the MLC leaves in deliveries and the realistic delivered doses during real time tracking cannot be calculated.

Given the limitations of current tracking methods, an ideal real time tracking method should have a few features: (1) it should account for the 3D deformable motion of the targets; (2) it should not require motion reproducibility; (3) it should be able to calculate the dose to patients during a realistic delivery with consideration of the interplay effect. Difficulties in developing such an ideal real time tracking method are twofold. First, measuring the real time 3D deformable motion of targets online exceeds the capability of current imaging techniques. The most commonly used imaging tool to measure the deformable motion of structures in today's radiotherapy is 4DCT. However, 4DCT cannot be acquired and reconstructed in real-time so that it is not suitable for online motion detection. Second, changing the preprogrammed 4D MLC leaf sequences online may break the synchronization between the 4D leaf sequences with the respiratory motion.

The first problem mentioned above may be addressed by using motion modeling. Modeling the 3D deformable motion of the tumor and the organs of a specific patient has been made possible with the rapid development of computational modeling techniques. Dynamic models of the lungs, the liver and the prostate have been developed[23–29] and used in radiation therapy applications.[30–33] Compared with 4DCT, 4D models have a few advantages including better temporal resolution and flexibility of motion pattern change so they may be used in guidance for real time tracking delivery.

The second problem, loss of synchronization between the 4D leaf sequences with online motion, could be solved by introducing a new tracking concept: predictive tracking. In real time tracking, the temporal information of the motion recorded prior to treatment is incorporated into the 4D leaf sequences so that online modification of the 4D sequences may break the synchronization between the leaf motion and the target motion. However, if the 4D sequencing step is skipped and the motion predicted online is directly used to modify the leaf positions from a 3D IMRT treatment plan without temporal information, loss of synchronization is less likely to happen. The method to directly convert a 3D IMRT plan to real-time delivery based on predicted motion is termed as predictive tracking. Figure 1 compares the workflow of "conventional" tracking, "real time" tracking, and "predictive" tracking.

Based on advanced motion modeling techniques and the predictive tracking concept, this study proposed a real time 4D IMRT planning method, called 4D model-based planning (4DMP). 4DMP is capable of accounting for the deformable motion of the target and critical structures in real time and calculating the delivered 4D doses with consideration of interplay effects during treatment deliveries. The feasibility of the 4DMP method was investigated in this study and the quality of 4DMP was compared with two other commonly used 4D treatment planning techniques: maximum intensity projection (MIP)34 and planning on individual phases (IP).[12]

II. MATERIALS AND METHODS

The 4DMP is a predictive tracking method consisting of two main steps: motion prediction and delivery beam adaptation. The basis of 4DMP is a dynamic virtual patient model, which is used to predict the motion, to adapt the delivery beams and to calculate the dose. Section II A introduces the techniques used to reconstruct a predictive virtual patient model from the 4DCT and the breathing curve of a patient. Section II B explains how to apply a virtual patient model for dose calculation, which is the basis of model-based treatment planning. Section II C then introduces the steps of 4DMP and compares it with MIP and IP.

II.A. Creation of a predictive dynamic virtual patient model

II.A.1. 4DCT acquisition

A 4DCT scan of a lung patient under quiet breathing was the main resource for the 4D model reconstruction. The CT images were acquired using a LightSpeed 16-slice CT (General Electric, WI) with a slice thickness of 2.5 mm. The scan

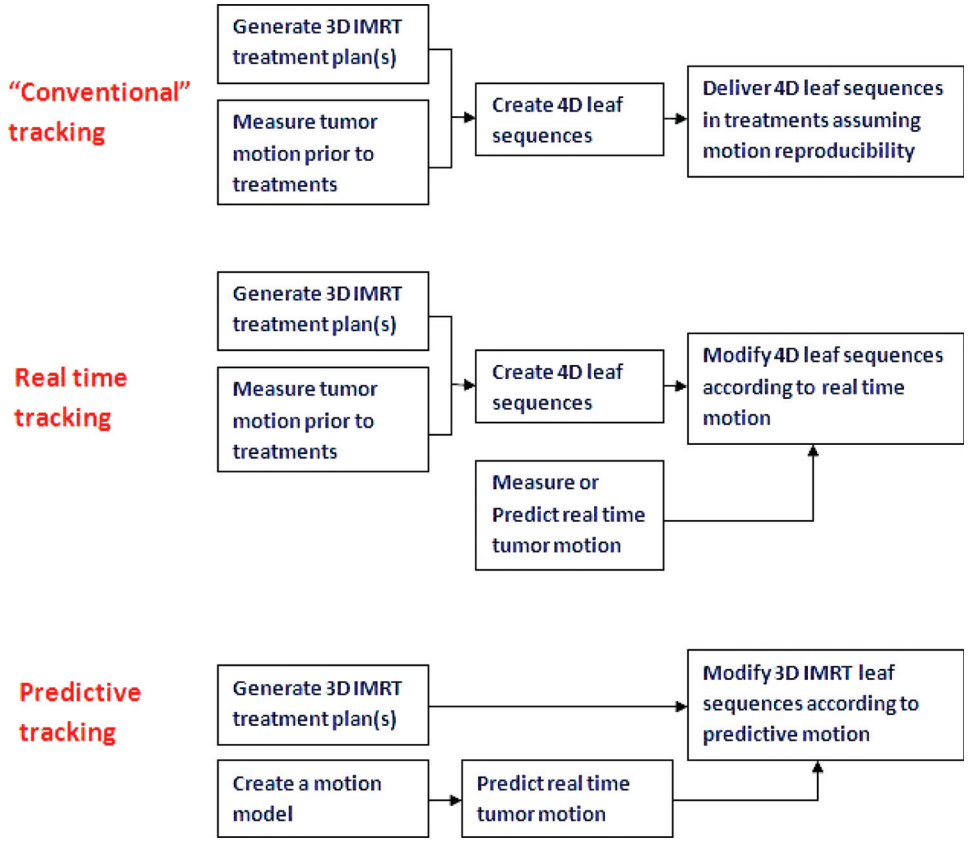

FIG. 1. Comparing the workflow of "conventional" tracking, real time tracking and predictive tracking.

took around 2 min. Respiratory signal was simultaneously acquired via the Varian real time respiratory position management (RPM) system (Varian Corporation, Palo Alto, CA). The CT images were then retrospectively sorted into 10 distinct phases (p0, p10, …, p90) corresponding to the phases of a respiratory cycle. P0 was defined as the end-inhale phase and p50 was the end-exhale phase. A single clinician segmented the gross tumor volume (GTV) and the organs at risk (OAR) on all phases. These contours were used as the "gold standard" for model reconstruction.

A "reference phase" was selected from the ten phases for model reconstruction and treatment planning. Considering that the end-inhale phase p0 is commonly the most stable phase, p0 was chosen as the reference phase. The mean amplitude of the breathing curve recorded at 4DCT acquisition was 1.0 cm and the mean period was 4.4 s.

II.A.2. 3D whole body NURBS model reconstruction

Contours of structures in the reference phase were converted to a three-dimensional (3D) whole body non-uniform rational B-spline (NURBS) model33 in two main steps:

(1) **Polygonzation**. For each structure, control points were automatically sampled from the original contours using an in-house code based on MATLAB.[35] A polygon of the structure was then formed by the control points. The code was designed to maintain the volume and the shape of the polygon the same as those of the original contours while keeping the number of control points as few as possible to reduce computation time.

(2) **Conversion to NURBS surfaces**. The structure polygons were then converted to three- degree NURBS surfaces using NURBS toolbox of MATLAB. Figure 2(a) compares the original contours, the polygon and the NURBS surface for the right lung. A 3D whole body model was then created as a collection of the 3D NURBS surfaces of the tumor and other organs at the reference phase.

II.A.3. Extending the 3D model to a 4D model based on 4DCT

The 3D whole body model developed on the end-inhale phase was propagated to other phases using the structure contours delineated on those phases. The 3D models of the tumor and other organs were transformed individually by shifting the control points forming the models so that the transformed models matched the structure contours on another phase. For a structure experiencing mainly translocation and rotation, such as the kidneys, the structure was treated as an entity in transformation. For a structure experiencing deformation, such as lungs and tumor, control points of structures were transformed individually. A procedure called "optimized deformation" was developed to automatically transform organ models. The concept of

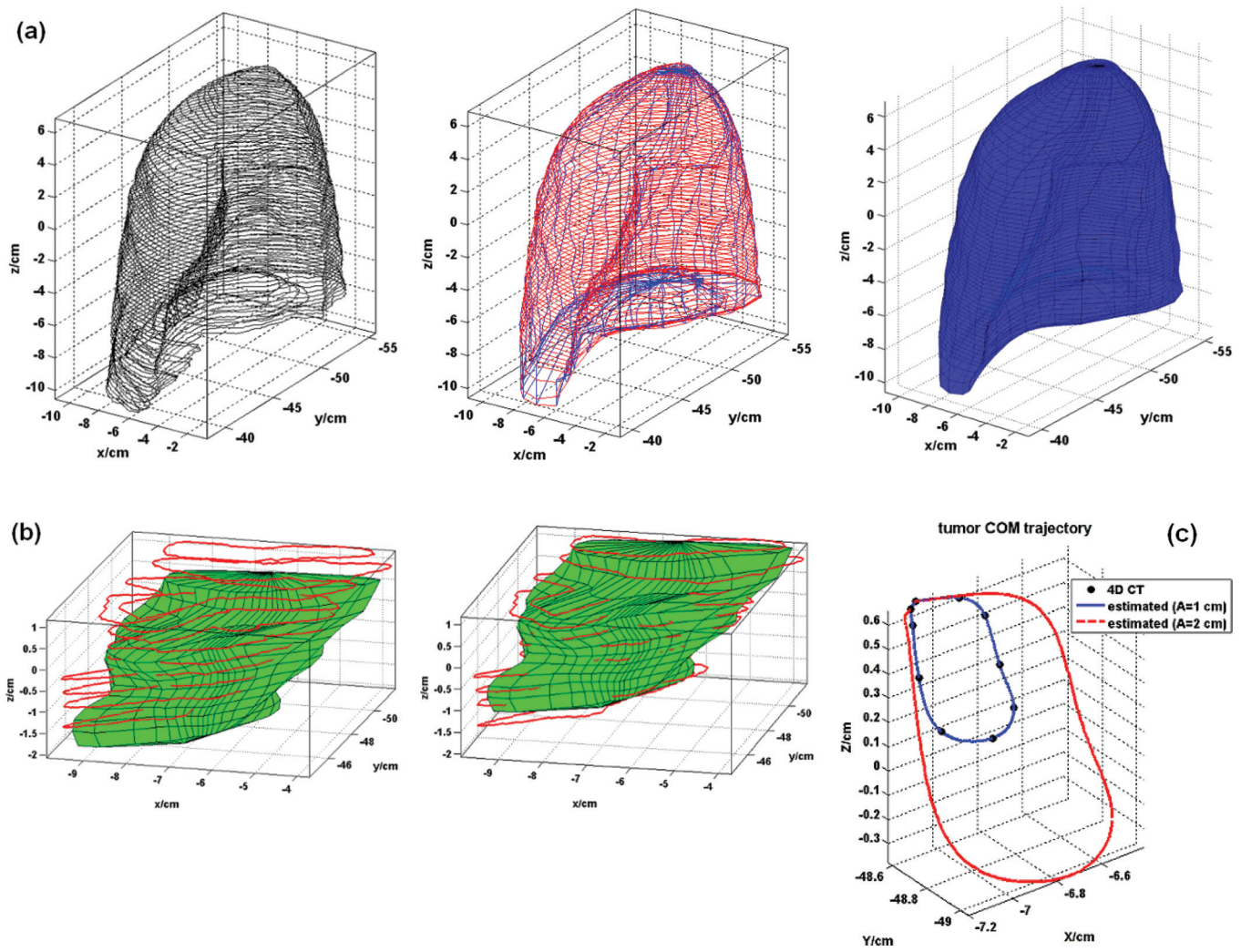

FIG. 2. Steps in the reconstruction of a 4D virtual patient model. (a) Reconstruction of 3D NURBS organ models. The original contours (left), the polygon (middle), and the NURBS surface (right) of the left lung in the reference phase are compared. (b) Extending a 3D organ model to 4D. The contours of the GTV (curves) are compared with the GTV models (surfaces). The left figure compares the GTV model in the end-inhale phase with the GTV contours in the end-exhale phase, and the right figure compares the GTV model deformed from the end-inhale phase to the end-exhale phase by optimized deformation with the GTV contours in the end-exhale phase. Percent volume overlap between the model and the contours was improved. (c) Extending the 4D model to different breathing patterns. The trajectories of the tumor's center of mass observed in 4DCT and estimated by Eq. (2) for breathing amplitudes of 1 and 2 cm are shown.

percent volume overlap (PVO) was used to evaluate how well two structures matched each other in geometry. PVO is calculated by Eq. (1), in which V_1 and V_2 are the volumes of two structures and V_{12} is the volume of their intersection. PVO considers the position, the volume, and the shape differences of two structures. An optimization algorithm was then used to search the optimal transformation of control points that will maximize the PVO between a structure model deformed from the reference phase and the contours of the structure on another phase. Optimization ends when the PVO between the two structures is larger than 95% or when the optimization time exceeds 1 h. Figure 2(b) compares the model of the GTV before and after deformation (surfaces) with the contours of the GTV at the end-exhale phase (curves). PVO was increased from 47 to 93% by optimized deformation. The displacement vector of each control point of each structure from the reference phase to other phases was then recorded.

$$PVO = \frac{V_{12}}{\sqrt{V_1 V_2}} \tag{1}$$

II.A.4. Extending the 4D model to different breathing patterns

A major limitation of 4DCT is that it only represents the motion of structures at the time of image acquisition, while the patient's breathing motion may vary largely from day to day. To overcome this limitation and achieve true real time treatment planning and delivery, we extended the 4D model to different breathing patterns, including regular periodic motion with different breathing amplitudes and irregular motion such as a realistic breathing curve. Equation (2) was used to estimate the displacement of the jth control point from the ith structure at a sampled time t for any breathing pattern. In this equation, $\vec{d}(i,j,t)$ is the displacement vector

of a control point and A_0 is the amplitude of breathing in 4DCT, which is also the mean amplitude of the breathing curve at 4DCT acquisition. In this study, $A_0 = 1\,cm$. $\theta(t)$ and $A(t)$ are the phase and the amplitude of a breathing curve at time t, and $\vec{f}$ stands for a three-degree B-spline interpolation between the phase of breathing and the displacement of the control point with breathing amplitude A_0. The displacement vectors of the control point at 10 phases $\vec{d}(i,j,p)$; $p = 0, 1...9$ were used to determine $\vec{f}$. This equation preserves the motion of structures observed in 4DCT including the hysteresis effect and allows extrapolation of motion range beyond 4DCT. By using this equation, it was assumed that the amplitude of internal organ motion was linearly proportional to the amplitude of the breathing curve. For a different internal-external relationship, the $A(t)/A_0$ term in Eq. (2) may be changed accordingly. Figure 2(c) compares the trajectory of the center of mass (COM) of the GTV observed in the 4DCT and the estimated GTV COM trajectories for breathing amplitude of 1 cm (same as the breathing amplitude of 4DCT) and 2 cm, respectively.

$$\vec{d}(i,j,t) = \frac{\vec{f}\left(\vec{d}(i,j,p), \theta(t)\right)(A(t))}{A_0}. \tag{2}$$

Structures in the thoracic and abdominal cavities are close to each other so when the structures are set in motion in a 4D model, the organ surfaces may "collide". To avoid the intersection of structures, a collision detection and correction algorithm was applied. Each structure was assigned an "elasticity coefficient" E so that when two structures collide with each other, the contact surfaces of both structures will deform. The extent of deformation is inversely proportional to the elasticity coefficient of the structure. Collision detection and correction is particularly important when extending the 4D model to motion range larger than that measured in 4DCT.

II.A.5. Predictive 4D virtual patient model

When a real-time breathing curve was used in Eq. (2) to estimate the motion of control points, the model was regarded as a "real-time" 4D virtual patient model. Furthermore, if combining the real-time motion with a motion prediction algorithm, the 4D model can be updated to "predictive" virtual human model and be used for predictive tracking. In this study, we assumed a prefect prediction algorithm was used so that the predicted breathing curve is exactly the same as the measured. Possible errors caused by this assumption will be discussed later.

II.B. Applying the 4D virtual patient models in dosimetry

II.B.1. Extracting deformation maps and 4DCT images from a dynamic model

To calculate doses from treatment plans to a 4D model, the model may be converted back to sets of 4DCT images using the 3D CT images of the reference phase and the deformation maps extracted from the 4D model. This procedure is termed as "model based registration". The motion/deformation of a NURBS organ model is represented by the displacement of control points defining the surface of the model. Due to the lack of motion information inside the organ model, it was assumed that the deformation of a structure propagates linearly from surface to inside. So, the deformation vector of a point within a structure is a function of the deformation vectors of the control points on the surface of the structure and the distances of the point to the surface, as shown by Eq. (3), in which N is the number of control points defining the structure; $\overrightarrow{d(x,y,z)}$ is the deformation vector of any point within this structure, $\vec{d}_i$ is deformation vector of ith control point and r_i is the distance of the point to that control point.

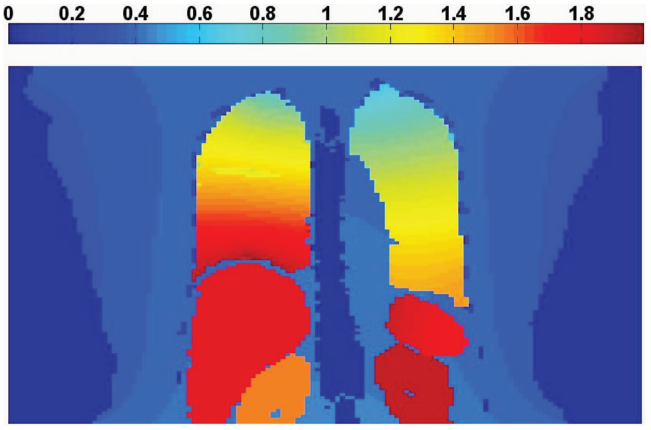

FIG. 3. The amplitude map of deformation (unit: cm) from the end-inhale phase to the end-exhale phase for a breathing amplitude of 2 cm.

$$\overrightarrow{d(x,y,z)} = \frac{\Sigma_{i=1}^{N} \frac{1}{r_i} \vec{d}_i}{\Sigma_{i=1}^{N} \frac{1}{r_i}} \tag{3}$$

Figure 3 shows the amplitude of the deformation map from the end-inhale phase to the end-exhale phase with breathing amplitude of 2 cm. The vertebral column is static during breathing. Structures such as the liver and the kidneys experience mainly translocation. Therefore, the amplitude of the deformation map inside these structures is uniform. The spleen experiences translocation and rotation, and the lungs and the tumor experience deformation; thus, the amplitude of the deformation map within these structures is nonuniform. For lungs, voxels near the diaphragm have larger deformation amplitudes than voxels near the apex. The deformation maps were used to create 4DCT images by deforming the 3D CT images at the reference phase.

II.B.2. Calculating the delivered 4D doses of IMRT plans while considering the realistic motion and the interplay effect

Model-based registration and CT image deformation allow dose calculation of IMRT treatments on a real time scale while taking into account the interplay effect. As illustrated in Fig. 4, each IMRT beam is composed of several segments. Given the synchronization of the measured breathing curve with the beam delivery, the dose delivered by each beam segment during a realistic IMRT treatment to the

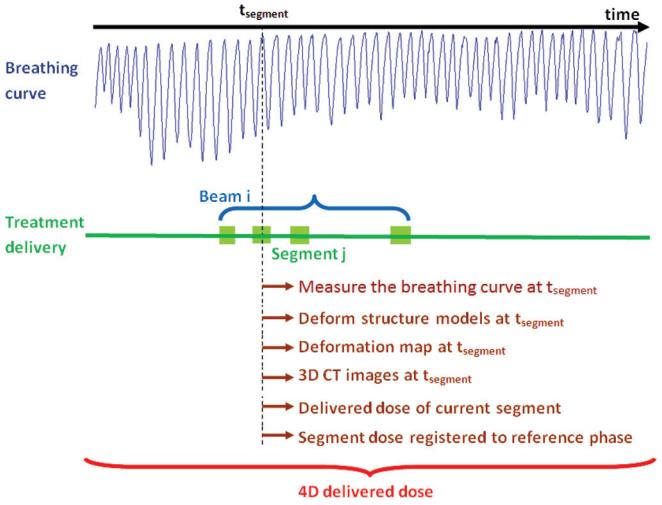

FIG. 4. Calculation of the delivered 4D doses of IMRT treatments with consideration of the realistic motion and the interplay effect. For each segment of the beams, the measured breathing curve at the time of segment delivery is used to deform the 4D model. The deformation map is extracted from the deformed model and the 3D CT images at the time of segment delivery are generated. Dose delivered by the segment to the 3D CT images is calculated and registered back to reference phase. The 4D delivered dose is then a summation of the segment doses.

deformed geometry can be calculated. For each segment of the beams, the measured breathing curve at the time of segment delivery is used to deform the 4D model. The deformation map is extracted from the deformed model and the 3D CT images at the time of segment delivery are generated. Dose delivered by the segment to the 3D CT images is calculated and registered back to the reference phase. The 4D delivered dose is then a summation of the segment doses. Based on the 4D models and the techniques to convert 4D models to sets of 4DCTs and deformation maps, a 4D treatment planning methodology, model-based 4D planning (4DMP), is proposed to provide a simple and efficient way of managing real time intrafraction motion.

II.C. 4D IMRT treatment planning based on 4D virtual patient models

II.C.1. 4DMP for regular motion

A 4D model provides information on changes in the morphology of the target and critical structures during breathing. A possible way to apply this information in 4D IMRT treatment planning is to apply the same morphology changes to treatment beams, called "morphology based 4D planning". The "direct aperture deformation" (DAD) method proposed by Yu *et al*. is one such technique.[36,37] In DAD planning, an IMRT treatment plan was first developed on the reference phase, and then the beam apertures of the plan were morphed to other phases based on the relative shape change of the target contours in the beam's eye view (BEV), called segment aperture morphing. For regular motion, 4DMP planning adopts the DAD concept except that the dynamic model of the planning target volume (PTV) instead of the contours of the PTV is used to deform the segments.

II.C.2. 4DMP for real-time motion

To account for motion during a realistic treatment delivery, 4DMP combines the segment morphing algorithm of DAD and a special predictive tracking delivery method. In real time 4DMP, an IMRT treatment plan is first developed on the reference phase and then propagated to a realistic delivery. As illustrated in Fig. 5, right after the delivery of one beam segment (time t), the system predicts the breathing curve of the patient with a prediction time, $t_{predict}$. The model of the PTV is then deformed according to the predicted breathing phase and amplitude. Both the PTV model at the reference phase and the deformed PTV model are projected to the BEV of the next segment, and the aperture of the next segment is then morphed according to the deformation of the PTV. After the segment morphing, MLC leafs are moved to form the shape of the next segment, which has been morphed previously, and the delivery of the next beam segment starts.

To ensure the synchronization of the delivery with the breathing motion, it is essential that the next beam segment is delivered at the predicted time, $t + t_{predict}$. In real time 4DMP, the delivery of the next beam segment was designed to start at $t + t_{predict} - 1/2MU/DR$ and finish at

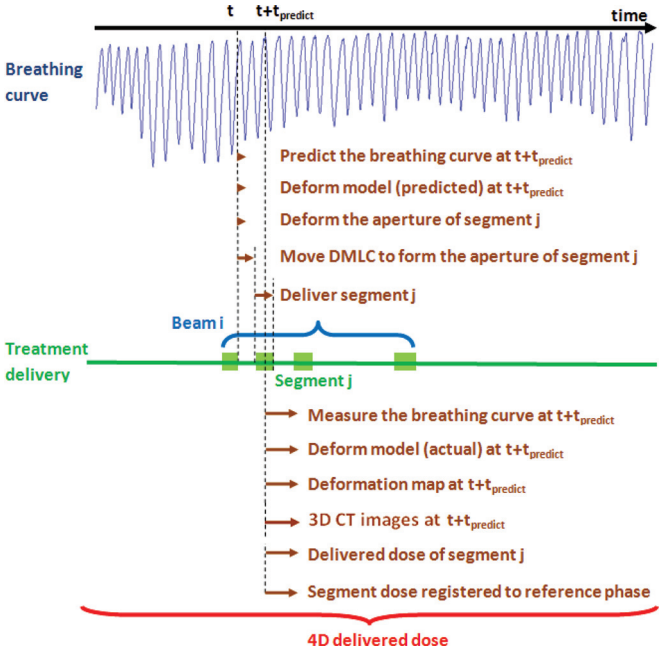

FIG. 5. Flow chart of real time 4DMP planning/delivery. Right after the delivery of one beam segment (time t), the system predicts the breathing curve of the patient for a prediction time $t_{predict}$. The model of the PTV is then deformed according to the predicted breathing phase and amplitude. Both the PTV model at the reference phase and the deformed PTV model are projected to the BEV of the next segment, and the aperture of the next segment is then morphed according to the deformation of the PTV. After the segment morphing, MLC leaves are moved to form the shape of the next segment, which has been morphed previously, and the delivery of the next beam segment starts. To calculate the 4D delivered dose of real-time 4DMP, for each segment of the beams, the measured breathing curve at the time of segment delivery is used to deform the 4D model. The deformation map is extracted from the deformed model and the 3D CT images at the time of segment delivery are generated. Dose delivered by the segment to the 3D CT images is calculated and registered back to reference phase. The 4D delivered dose is then a summation of the segment doses.

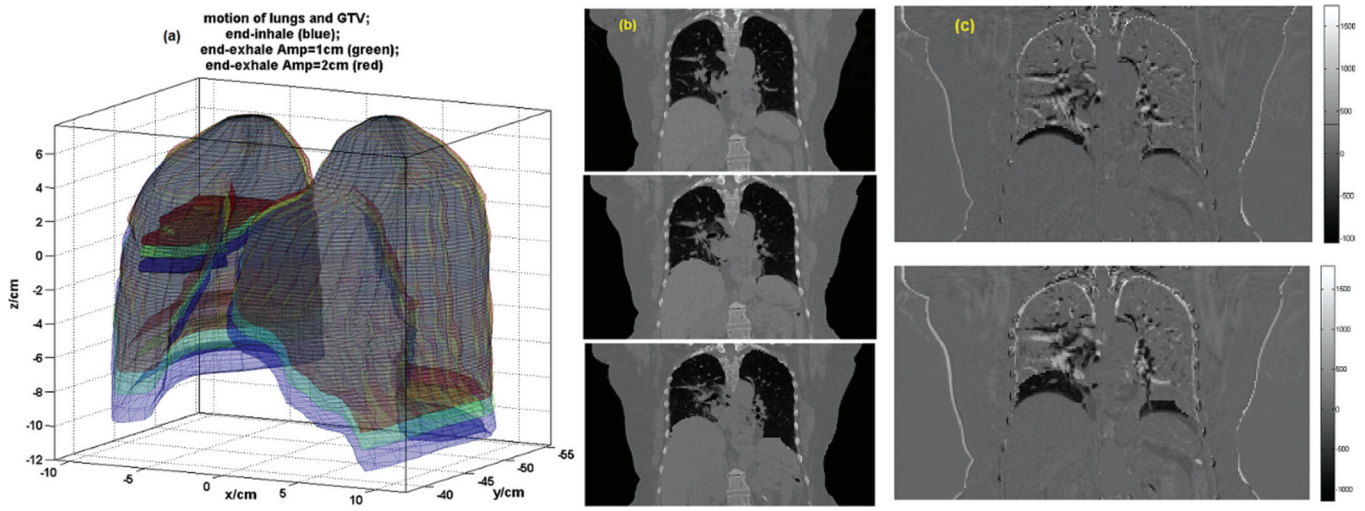

FIG. 6. 4D model at the end-inhale and the end-exhale phases for breathing amplitudes of 1 cm and 2 cm and the corresponding CT images. (a) lungs and GTV at the end-inhale phase and two end-exhale phases with breathing amplitude of 1 and 2 cm, respectively; (b) CT images at difference breathing phases; top: the end-inhale phase; middle: deformed CT images at the end-exhale phase with breathing amplitude of 1 cm; bottom: deformed CT images at the end-exhale phase with breathing amplitude of 2 cm; (c) difference of the CT images between the end-inhale and the end-exhale phases; upper: 1 cm breathing amplitude; lower: 2 cm breathing amplitudes.

$t + t_{predict} + 1/2MU/DR$, in which MU is the number of monitor units in the next beam segment and DR is the dose rate. The predicted time $t + t_{predict}$ is then right in the middle of the segment delivery. If we assume that the time for motion prediction, structure deformation, and aperture morphing is negligible, the leaves of MLCs have to move from the previous positions to the new positions within a time of $t_{predict} - 1/2MU/DR$ to maintain synchronization and avoid beam hold offs.

4DMP is a real time planning method that can account for the irregular, 3D deformable motion of the target during a realistic treatment delivery. It is also a very efficient planning/delivery technique because the number of segments in a real time 4DMP plan is the same as the 3D IMRT plan in the reference phase. The delivered 4D doses of 4DMP plans can be calculated during or after the real time 4DMP delivery. For each segment, the measured breathing phase and amplitude at the time of segment delivery are used to deform the models of structures, to extract the deformation maps and to create the deformed 3D CT images. The delivered dose of each segment is then calculated using the deformed CT images and the morphed segment aperture. Segment doses are registered back to the reference phase and the 4D delivered dose is the summation of all segment doses.

There are two determining factors affecting the success of a real time 4DMP delivery: the prediction time between segments and the residual motion within a segment. The prediction error increases as the prediction time increases, so a short prediction time is desirable. However, to make sure that the MLC leaves can travel from the positions of the previous segment to the positions of the next segment within the prediction time, it is desirable to have a large prediction time. As a compromise, we used a prediction time of 200 ms for arc IMRT plans in this study. The residual motion within a segment delivery is proportional to the time of segment delivery and thus inversely proportional to the dose rate. To reduce the residual motion, it is desirable to select a large dose rate. In this study, we used a dose rate of 1000 MU/min for treatment planning.

II.C.3. Comparing 4DMP with MIP and IP under regular motion

To evaluate the quality of 4DMP plans, we compared the 4DMP with MIP and IP. The three 4D treatment planning strategies were compared for rotational (arc) IMRT plans. Both MIP and IP plans assume the reproducibility of the breathing pattern and ignore the interplay effect, so the quality of 4DMP plans was first compared with MIP and IP based on these two assumptions. The 4D virtual patient model was converted to two sets of 4DCT images, one with breathing amplitude of 1 cm and the other with a 2 cm breathing amplitude. Each 4DCT consist of 10 phases with equal time weightings. Structure contours on each phase and the deformation maps from the reference phase to other phases were extracted from the 4D model. The 4DCT images and the structure contours were imported into Pinnacle[3] treatment planning system (Version 9.0, Philips, Fitchburg, WI) for IMRT treatment planning.

TABLE I. Motion/deformation of the GTV at different breathing amplitudes characterized by the volume of tumor, the movement of center of mass (COM) and the percent volume overlap (PVO) between the end-inhale phase and the end-exhale phase.

	End-inhale	End-exhale (breathing amplitude = 1 cm)	End-exhale (breathing amplitude = 2 cm)
Volume (cc)	21.05	19.13	18.19
Movement of COM	–	0.6 cm	1.3 cm
PVO	–	47%	23%

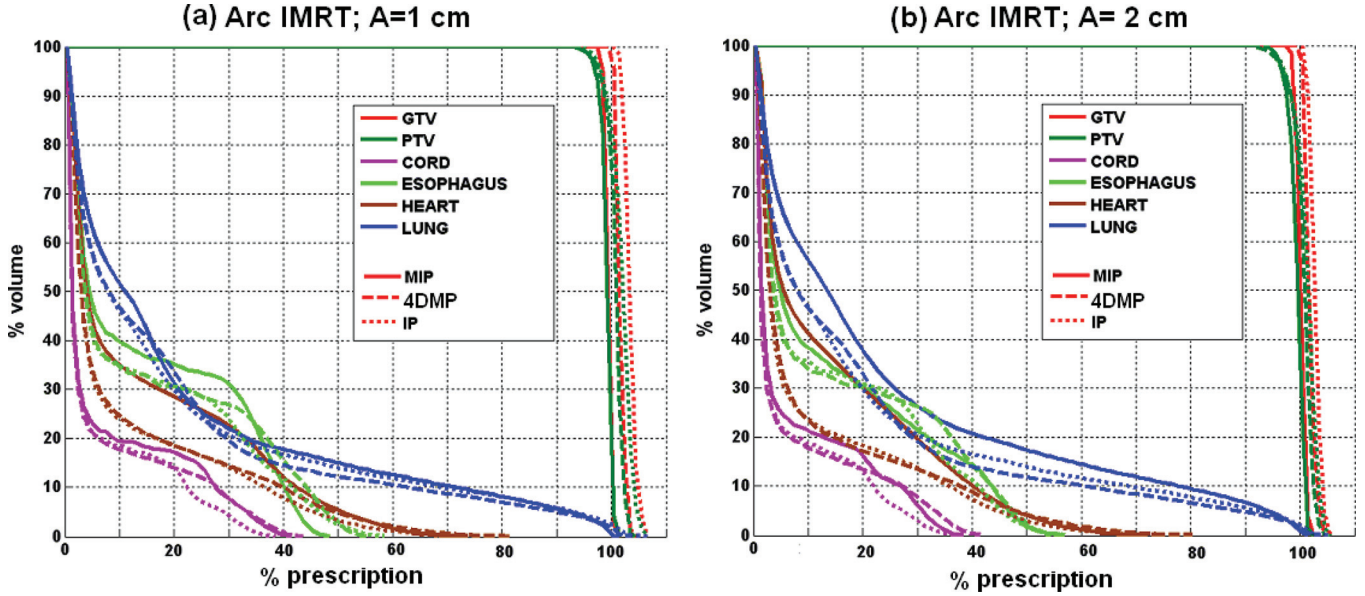

FIG. 7. Comparing the 4D composite DVHs of structures between MIP, IP and 4DMP 4D planning methods for (a) arc IMRT plans with breathing amplitude of 1 cm and (b) arc IMRT plans with breathing amplitude of 2 cm.

For IP planning, the treatment plans were developed independently on each of 10 phases. In each phase, the PTV was defined by expanding the GTV of this phase with a 0.5 cm set-up margin. 60 Gy was prescribed to the mean dose to the PTV in 30 fractions for all phases. 4DMP planning used the same margin and prescription as IP planning. A treatment plan was developed on the reference phase and then propagated to other phases. For 4DMP and IP planning, the doses on all 10 phases were registered back to the reference phase using the deformation maps extracted from model, and the 4D composite doses of IP and 4DMP plans were calculated by averaging the deformed dose maps. The 4D composite dose volume histograms (DVHs) for the GTV, PTV and critical structures were calculated using the 4D composite dose and the structure contours in the reference phase.

For MIP planning, the treatment plan was developed using the mean CT image with the internal target volume (ITV) defined as the union of the GTVs in all 10 phases. The PTV was defined by expanding the ITV with a 0.5 cm set-up margin. The prescription was the same as in the 4DMP and IP plans. To calculate the 4D composite dose distributions of a MIP IMRT plan, the MIP plan for the mean CT image was extracted and then imported to the images of all 10 phases. Dose calculation was performed on individual phases, and the 4D doses and DVHs were calculated using the same method as IP and 4DMP plans.

TABLE II. Comparing the coverage of target PTV V_{97}, the lung V_{20} and the maximum dose D_{max} to spinal cord for three 4D planning strategies under regular motion.

		$A=1$ cm		$A=2$ cm
PTV V_{97}/%	MIP	93.4	MIP	91.1
	IP	97.2	IP	93.8
	4DMP	96.1	4DMP	93.6
Lung V_{20}/%	MIP	20.0	MIP	23.9
	IP	19.0	IP	18.8
	4DMP	17.0	4DMP	16.7
Cord D_{max}/Gy	MIP	24.9	MIP	23.0
	IP	22.8	IP	22.6
	4DMP	25.7	4DMP	24.8

II.C.4. Comparing 4DMP with MIP and IP under realistic irregular motion

During a realistic IMRT treatment delivery, the target may move beyond the range seen in 4DCT, and the interplay between the motion of MLCs and structures may cause further deviation of the delivered dose from the planned dose. Therefore, to compare 4DMP with MIP and IP under

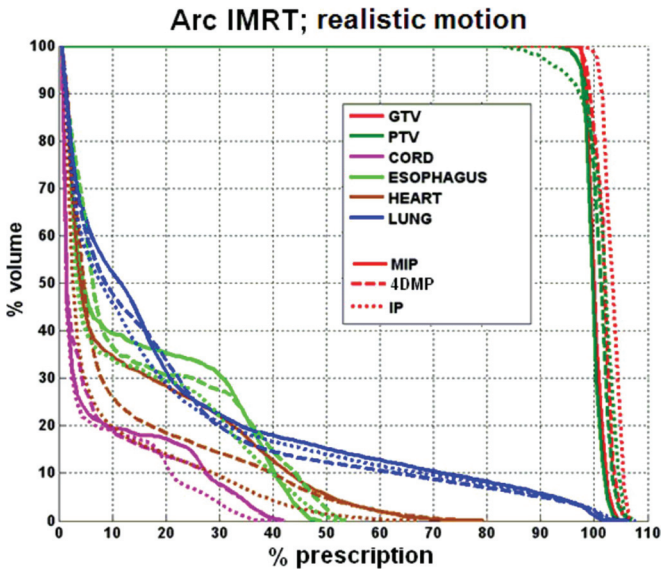

FIG. 8. Comparison of the 4D composite DVHs between the three 4D treatment planning methods under realistic motion.

TABLE III. Comparing the coverage of target PTV V_{97}, the lung V_{20} and the maximum dose D_{max} to spinal cord for three 4D planning strategies under realistic motion.

		Realistic motion
PTV V_{97}/%	MIP	90.4
	IP	89.4
	4DMP	94.1
Lung V_{20}/%	MIP	20.1
	IP	19.0
	4DMP	17.5
Cord D_{max}/Gy	MIP	24.7
	IP	23.9
	4DMP	26.8

realistic motion, it is necessary to calculate the "delivered 4D doses" while taking into account the interplay effect.

A real time 4DMP treatment plan was developed for the 4D model. The delivery of the first segment was assumed to start at the beginning of the breathing curve. The delivered 4D doses of the arc 4DMP plans were calculated using the method shown in Fig. 5. Though MIP and IP plans were not designed for delivery with irregular motion, we were still able to estimate the delivered 4D doses of MIP and IP plans using the 4D virtual patient model, using the method shown in Fig. 4, as long as the synchronization of beam delivery with the real time breathing curve was known. For MIP plans, the delivery of the first segment was also assumed to start at the beginning of the breathing curve. The times between the segments were estimated by assuming a constant leaf travel velocity of 2.5 cm/s. An IP plan includes 10 IMRT plans developed on different phases. To determine the synchronization of the IP plan deliveries with the breathing curve, we assumed that the first segments of all 10 plans were delivered in the first cycle of breathing to the corresponding phase. Leaf speed constraints were ignored. Assuming the number of segments of the 10 IMRT plans is $\{Ni\}$, where $i = 1, 2,\ldots, 10$, the number of breathing cycles required to finish an IP plan delivery was the maximum of $\{Ni\}$. This method assumed that all the segments of the 4D IP plan were delivered to the correct phase. For MIP and IP plans, any deviation of the delivered 4D doses from the planned 4D doses is the result of breathing irregularity and the interplay effect.

III. RESULTS

III.A. Motion features of the 4D virtual patient model

Figure 6(a) shows the motion of the lungs and the GTV. The organ surfaces were plot in blue for the end-inhale phase, green for the end-exhale phase with breathing amplitude of 1 cm and red for the end-exhale phase with breathing amplitude of 2 cm. Figure 6(b) compares the CT images at the end-inhale phase (top figure), the end-exhale phase with breathing amplitude 1 cm (middle figure), and the end-exhale phase with breathing amplitude 2 cm (bottom). The difference of CT images at end-inhale and end-exhale phases were shown in Fig. 6(c). The upper figure is the difference at breathing amplitude of 1 cm and the lower figure is the difference at breathing amplitude of 2 cm. The largest CT number changes were observed near the diaphragm, at the skin-air interface, at the ribs and at the tumor location. Abdominal organs also experienced large motion as shown by the deformation map in Fig. 3(b). However, because of the relatively low contrast in the abdomen, the change of CT number was not as large as in the thoracic region.

The motion of the GTV, quantified by the change of its volume and center of mass (COM) and the percent volume overlap (PVO) between the end-inhale phase and the end-exhale phase is shown in Table I.

III.B. Dosimetric comparison of different 4D planning strategies under regular motion

Figure 7 compares the 4D composite DVHs for the target and critical structures of three 4D treatment planning methods for (a) arc IMRT plans with breathing amplitude of 1 cm and (b) arc IMRT plans with breathing amplitude of 2 cm.

TABLE IV. Comparing the volumes and the COMs of structures between the dynamic model and the original contours for the end-inhale phase and the end-exhale phase. The percent differences of the volumes and the distances of COMs are listed.

	End-inhale (P0)				End-exhale (P50)			
		COM/mm				COM/mm		
Organs	Volume/%	*x*	*y*	*z*	Volume/%	*x*	*y*	*z*
PTV	−0.8	−0.04	−0.02	0.00	−0.7	0.04	0.00	−0.01
Esophagus	2.1	−1.48	0.62	1.57	−2.2	−0.30	−0.15	0.30
Heart	−3.2	0.15	0.05	−0.30	−3.2	−1.02	−0.16	−0.37
Left lung	−1.1	−0.67	−1.22	−0.20	−1.6	−0.62	0.61	0.50
Right lung	3.2	−0.36	0.42	0.05	2.9	−0.26	1.13	−2.71
Left kidney	−0.5	0.15	−0.19	0.12	−4.8	0.14	−0.18	−0.02
Right kidney	−4.4	0.13	−0.24	0.10	−6.3	0.17	0.31	0.25
Liver	−2.0	−0.33	−0.14	0.00	−1.9	−0.30	0.01	−0.12
Spinal cord	−0.5	0.10	−0.40	0.30	−0.5	0.10	−0.40	0.30
Spleen	−1.5	0.06	0.00	−0.06	−1.8	0.10	−0.10	−0.10
Stomach	−0.2	0.52	−0.48	0.35	−5.1	1.09	0.19	0.73

TABLE V. Maximal leaf velocities between the segments of real time 4DMP delivery.

Plan	# of beams and segments	Prediction (time/ms)	0–1 (cm/s)	1–2 (cm/s)	2–3 (cm/s)	3–4 (cm/s)	4–5 (cm/s)	>5 (cm/s)
4DMP	1 beam, 91 segments	200	15	17	48	8	2	0

Table II quantitatively compares the coverage of the target PTV, V_{97}, defined as the percent of the PTV volume receiving no less than 97% of the prescription dose; the lung V_{20}, defined as the percent volume of lungs receiving no less than 20 Gy (in 30 fractions); and the maximum dose D_{max} to spinal cord. Coverage of the target was similar for all three 4D planning techniques and for both breathing amplitudes. MIP plans had the highest normal tissue doses. Normal tissue sparing was comparable between the 4DMP plans and the IP plans; lung dose was lowest in the 4DMP plans but doses to other critical structures such as the spinal cord, the heart and the esophagus were lower for IP plans.

Changing the breathing amplitude affected the plan quality for all three 4D planning strategies. For MIP plans, the target coverage remained the same when the amplitude of breathing increased from 1 to 2 cm, but the doses to normal structures, especially to the lungs, were largely increased. For IP and 4DMP plans, the normal tissue doses were similar but the coverage of target was slightly reduced when breathing amplitude increased.

Overall, under regular motion, 4DMP improved normal tissue sparing compared with MIP plans with similar target coverage at small breathing amplitudes and slightly reduced target coverage at large breathing amplitudes. Compared with IP plans, 4DMP gave comparable plan quality with reduced planning workload.

III.C. Dosimetric comparison of different 4D planning strategies under realistic treatment delivery

Figure 8 compares the 4D composite DVHs for the target and critical structures of three 4D treatment planning methods under realistic delivery conditions. Table III compares the PTV V_{97}, the lung V_{20}, and the D_{max} to spinal cord. Under realistic motion, the target coverage of real time 4DMP was comparable to MIP and superior to IP. PTV V_{97} was 90.4% for the MIP plan, 88.6% for the IP plan, and 94.1% for the 4DMP plan. Normal tissue sparing for real time 4DMP was superior to MIP and similar to IP. Lung V_{20} was 20.1% for the MIP plan, 17.8% for the IP plan, and 17.5% for the 4DMP plan. For a realistic breathing pattern, real time 4DMP offered better plan quality than MIP and IP methods.

IV. DISCUSSION

IV.A. The accuracy of the dynamic virtual human model

Modeling accuracy is essential in the model-based planning technique. In this study, to verify the geometric accuracy of the dynamic virtual patient model, we compared the models with the original contours of organs at difference phases. Table IV lists the percent difference of volumes and the distances of COMs at the end-inhale phase and the end-exhale phase. For most of the structures, the percent difference of the volumes was within 5% and the distances of the COMs at x, y, and z directions were within 1 mm. Increasing the number of sampled control points could further reduce the volume and COM differences on the expense of longer sampling and model reconstructing time.

Table IV verifies that the dynamic model matches the structure contours in geometry. However, because the model was reconstructed based on the contours and verified against the contours, it is only as accurate as the contours. Any uncertainties in the manual contouring process[38] will decrease the accuracy of motion modeling and thus affecting the quality of 4DMP planning and delivery. Besides the contouring error, another main source of uncertainties in motion modeling is the internal–external correlation. In this study, it was assumed that the amplitude of the internal structure motion was linearly proportional to the amplitude of the breathing curve, measured externally by RPM system. However, this correlation has been debated by some researchers.[39,40]

So to use the 4DMP technique in clinical applications, the motion modeling accuracy has to be improved. A possible way is to incorporate physiological information such as air pressure and air flow into modeling to achieve a better understanding of the motion of the tumor and other internal organs.[23,29] Physiological models may have more realistic representation of organ geometries than contours and show more precise internal–external correlation than linear assumption thus is more suitable for 4DMP than simple geometry models.

IV.B. The rationale to use model based registration

While motion modeling determines the precision of tracking, the accuracy of 4D dose calculation is also dependent on the dose registration algorithm used. Most previous 4D planning studies have used deformable image registration algorithms to calculate 4D dose. But this study developed a new algorithm: model based registration. The reason is that, for motion range beyond that of 4DCT, it is not feasible to generate an image based deformation map, so model based registration is the only way to estimate the deformation map under a realistic delivery. Besides that, model based registration also have a few advantages than 4DCT: it is faster, not susceptible to image artifacts, and equally reliable in high and low contrast regions.

A major concern of model based registration is its accuracy. Model based registration assumes that motion propagates linearly from the surface of a structure to inside, which may not be true for some structures such as the lungs.

TABLE VI. Residual motion within delivery of segments for real time 4DMP.

Plan	# of beams and segments	Dose rate/MU/min	0–1 (mm)	1–2 (mm)	2–3 (mm)	3–4 (mm)	4–5 (mm)	>5 (mm)
4DMP	1 beam, 91 segments	600	32	50	7	2	0	0
		1000	77	14	0	0	0	0

However, the linear assumption ensures that a voxel inside a structure remains inside after deformation and this feature is desirable in calculating the 4D DVHs to the PTV and organs of risks. To improve the accuracy of model based registration, a possible solution is to upgrade the surface based geometry models to volume based geometry models which would give the deformation in 3D volume directly.

IV.C. The deliverability of the real time 4DMP plans

A common problem of tracking methods is the deliverability of the plans, when machine constraints such as the MLC leaf travel speed is considered. We calculated the maximum leaf speed between the segments of the real-time 4DMP plan. Table V summarizes the results. Most of the maximum leaf velocities lie within 3 cm/s and all leaf velocities lie within 5 cm/s. So, the deliverability of the real time 4DMP plans was demonstrated for the prediction time used in this study.

IV.D. The residual motion of the real time 4DMP plans

The residual motion within the delivery of a beam segment was determined by the MU of the beam segment, the dose rate used and the gradient of the breathing curve at the time of segment delivery. Table VI summarizes the residual motion of the breathing curve for the arc 4DMP plans with dose rate of 600 and 1000 MU/min, respectively. Apparently a larger dose rate resulted in less residual motion. For the dose rate used in this study (1000 MU/min), all segments had residual motion lower than 2 mm, and most segments had residual motion lower than 1 mm. This residual motion is lower than for typical gating deliveries.[41]

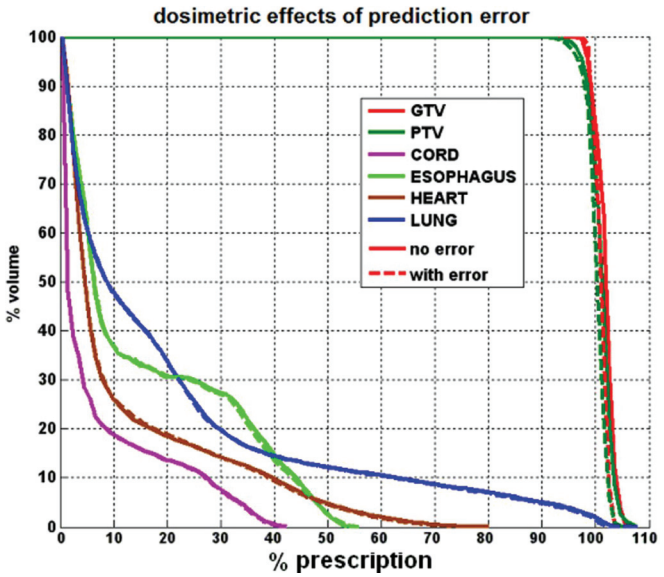

FIG. 9. Dosimetric effect of prediction errors in real time 4DMP planning/delivery.

IV.E. The dosimetric effects of prediction error

To evaluate the dosimetric effect of possible prediction errors, we use the arc real time 4DMP plan as an example. Previous studies have shown that current prediction filters can predict motion with an accuracy of 2 mm for a prediction time of 0.57 s.[42] Assuming the error of prediction is a Gaussian distribution with standard deviation of 2 mm, we generated a real time 4DMP plan with such prediction error and compared the 4D composite dose with the planned 4D composite dose in Fig. 9. We found that the introduction of prediction error does not change the target coverage or normal tissue doses significantly.

V. SUMMARY

This paper proposed a novel 4D real time treatment planning method (4DMP) based on dynamic virtual patient models and a concept called predictive tracking. The 4DMP is capable of managing the real time 3D deformable motion of target without increasing the workload of treatment planning or time of delivery. For a regular breathing pattern, 4DMP gave similar plan quality compared with IP and better normal tissue sparing than MIP plans. For an irregular motion pattern with consideration of the interplay effect in beam delivery, 4DMP gave better plan quality than IP and MIP. The deliverability of 4DMP plans was demonstrated, and it was found that the possible errors caused by prediction uncertainties and residual motion within segment delivery do not affect the quality of 4DMP plans significantly. This initial study showed that the application of sophisticated virtual patient models may greatly benefit radiation therapy treatment planning and delivery. More patient studies are pending to validate the efficacy of the model-based planning method for various patient geometries and motion patterns.

ACKNOWLEDGMENTS

The authors would like to gratefully acknowledge the funding support from NIH/NLM Grant No. R01LM009362 and Patricia Tynan for her help in proofreading this paper.

[a]Author to whom correspondence should be addressed. Electronic mail: bingqi@med.umich.edu

[1]P. J. Keall, G. S. Mageras, J. M. Balter, R. S. Emery, K. M. Forster, S. B. Jiang, J. M. Kapatoes, D. A. Low, M. J. Murphy, B. R. Murray, C. R. Ramsey, M.B. Van Herk, S. S. Vedam, J. W. Wong, and E. Yorke, "The management of respiratory motion in radiation oncology report of AAPM Task Group 76," Med. Phys. **33**, 3874–3900 (2006).

[2]M. J. Murphy, "Tracking moving organs in real time," Semin. Radiat. Oncol. **14**, 91–100 (2004).
[3]S. Webb, "The effect on IMRT conformality of elastic tissue movement and a practical suggestion for movement compensation via the modified dynamic multileaf collimator (dMLC) technique," Phys. Med. Biol. **50**, 1163–1190 (2005).
[4]L. Papieza, "DMLC leaf-pair optimal control of IMRT delivery for a moving rigid target," Med. Phys. **31**, 2742–2754 (2004).
[5]D. McQuaid and S. Webb, "IMRT delivery to a moving target by dynamic MLC tracking: Delivery for targets moving in two dimensions in the beam's eye view," Phys. Med. Biol. **51**, 4819–4839 (2006).
[6]D. McQuaid, M. Partridge, J. R. Symonds-Tayler, P. M. Evans, and S. Webb, "Target-tracking deliveries on an Elekta linac: A feasibility study," Phys. Med. Biol. **54**, 3563–3578 (2009).
[7]R. George, Y. Suh, M. Murphy, J. Williamson, E. Weiss, and P. Keall, "On the accuracy of a moving average algorithm for target tracking during radiation therapy treatment delivery," Med. Phys. **35**, 2356–2365 (2008).
[8]T. Neicu, H. Shirato, Y. Seppenwoolde, and S. B. Jiang, "Synchronized moving aperture radiation therapy (SMART): average tumour trajectory for lung patients," Phys. Med. Biol. **48**, 587–598 (2003).
[9]Y. Suh, A. Sawant, R. Venkat, and P. J. Keall, "Four-dimensional IMRT treatment planning using a DMLC motion-tracking algorithm," Phys. Med. Biol. **54**, 3821–3835 (2009).
[10]Y. Liang, H. Xu, J. Yao, Z. Li, and W. Chen, "Four-dimensional intensity-modulated radiotherapy planning for dynamic multileaf collimator tracking radiotherapy," Int. J. Radiat. Oncol., Biol., Phys. **74**, 266–274 (2009).
[11]The dimensionality of the tumor motion was in reference to the beam direction and the motion of DMLC leaves. 1D: tumor moves parallel to the DMLC leaf motion; 2D: tumor moves both parallel and perpendicular to the DMLC leaf motion in the beam's eye view (BEV); 3D: tumor moves in all three directions.
[12]P. J. Keall, S. Joshi, S. S. Vedam, J. V. Siebers, V. R. Kini, and R. Mohan, "Four-dimensional radiotherapy planning for DMLC-based respiratory motion tracking," Med. Phys. **32**, 942–951 (2005).
[13]G. D. Hugo, J. Liang, J. Campbell, and D. Yan, "On-line target position localization in the presence of respiration: a comparison of two methods," Int. J. Radiat. Oncol., Biol., Phys. **69**, 1634–1641 (2007).
[14]D. Ruan, J. A. Fessler, J. M. Balter, and J. J. Sonke, "Exploring breathing pattern irregularity with projection-based method," Med. Phys. **33**, 2491–2499 (2006).
[15]D. Ruan, J. A. Fessler, J. M. Balter, and P. J. Keall, "Real-time profiling of respiratory motion: Baseline drift, frequency variation and fundamental pattern change," Phys. Med. Biol. **54**, 4777–4792 (2009).
[16]S. Vedam, A. Docef, M. Fix, M. Murphy, and P. Keall, "Dosimetric impact of geometric errors due to respiratory motion prediction on dynamic multileaf collimator-based four-dimensional radiation delivery," Med. Phys. **32**, 1607–1620 (2005).
[17]D. Ruan, J. A. Fessler, and J. M. Balter, "Real-time prediction of respiratory motion based on local regression methods," Phys. Med. Biol. **52**, 7137–7152 (2007).
[18]D. Ruan and P. Keall, "Online prediction of respiratory motion: Multidimensional processing with low-dimensional feature learning," Phys. Med. Biol. **55**, 3011–3025 (2010).
[19]C. Ozhasoglu, C. B. Saw, H. Chen, S. Burton, K. Komanduri, N. J. Yue, S. M. Huq, and D. E. Heron, "Synchrony–cyberknife respiratory compensation technology," Med. Dosim. **33**, 117–123 (2008).
[20]A. Sawant, R. Venkat, V. Srivastava, D. Carlson, S. Povzner, H. Cattell, and P. Keall, "Management of three-dimensional intrafraction motion through real-time DMLC tracking," Med. Phys. **35**, 2050–2061 (2008).
[21]A. Sawant, R. L. Smith, R. B. Venkat, L. Santanam, B. Cho, P. Poulsen, H. Cattell, L. J. Newell, P. Parikh, and P. J. Keall, "Toward submillimeter accuracy in the management of intrafraction motion: the integration of real-time internal position monitoring and multileaf collimator target tracking," Int. J. Radiat. Oncol., Biol., Phys. **74**, 575–582 (2009).
[22]B. Y. Yi, S. Han-Oh, F. Lerma, B. L. Berman, and C. Yu, "Real-time tumor tracking with preprogrammed dynamic multileaf-collimator motion and adaptive dose-rate regulation," Med. Phys. **35**, 3955–3962 (2008).
[23]D. A. Low, P. J. Parikh, W. Lu, J. F. Dempsey, S. H. Wahab, J. P. Hubenschmidt, M. M. Nystrom, M. Handoko, and J. D. Bradley, "Novel breathing motion model for radiotherapy," Int. J. Radiat. Oncol., Biol., Phys. **63**, 921–929 (2005).
[24]D. Yang, W. Lu, D. A. Low, J. O. Deasy, A. J. Hope, and I. El Naqa, "4D-CT motion estimation using deformable image registration and 5D respiratory motion modeling," Med. Phys. **35**, 4577–4590 (2008).
[25]K. K. Brock, S. J. Hollister, L. A. Dawson, and J. M. Balter, "Technical note: Creating a four-dimensional model of the liver using finite element analysis," Med. Phys. **29**, 1403–1405 (2002).
[26]J. M. Hensel, C. Menard, P. W. Chung, M. F. Milosevic, A. Kirilova, J. L. Moseley, M. A. Haider, and K. K. Brock, "Development of multiorgan finite element-based prostate deformation model enabling registration of endorectal coil magnetic resonance imaging for radiotherapy planning," Int. J. Radiat. Oncol., Biol., Phys. **68**, 1522–1528 (2007).
[27]T. N. Nguyen, J. L. Moseley, L. A. Dawson, D. A. Jaffray, and K. K. Brock, "Adapting population liver motion models for individualized online image-guided therapy," *Conference Proceedings IEEE Engineering in Medicine and Biology Society* (EMBS 20th Annual International Conference of the IEEE, Vancouver, Canada, 2008), pp. 3945–3948.
[28]T. N. Nguyen, J. L. Moseley, L. A. Dawson, D. A. Jaffray, and K. K. Brock, "Adapting liver motion models using a navigator channel technique," Med. Phys. **36**, 1061–1073 (2009).
[29]J. Eom, G. X. Xu, S. De, and C. Shi, "Predictive modeling of lung motion over the entire respiratory cycle using measured pressure-volume data, 4DCT images and finite-element analysis," Med. Phys. **37**, 4389–4400 (2010).
[30]Q. Zhang, A. Pevsner, A. Hertanto, Y. C. Hu, K. E. Rosenzweig, C. C. Ling, and G. S. Mageras, "A patient-specific respiratory model of anatomical motion for radiation treatment planning," Med. Phys. **34**, 4772–4781 (2007).
[31]J. Zhang, G. X. Xu, C. Shi, and M. Fuss, "Development of a geometry-based respiratory motion-simulating patient model for radiation treatment dosimetry," J. Appl. Clin. Med. Phys. **9**, 2700 (2008).
[32]R. Colgan, J. McClelland, D. McQuaid, P. M. Evans, D. Hawkes, J. Brock, D. Landau, and S. Webb, "Planning lung radiotherapy using 4D CT data and a motion model," Phys. Med. Biol. **53**, 5815–5830 (2008).
[33]R. McGurk, J. Seco, M. Riboldi, J. Wolfgang, P. Segars, and H. Paganetti, "Extension of the NCAT phantom for the investigation of intra-fraction respiratory motion in IMRT using 4D Monte Carlo," Phys. Med. Biol. **55**, 1475–1490 (2010).
[34]R. W. Underberg, F. J. Lagerwaard, B. J. Slotman, J. P. Cuijpers, and S. Senan, "Use of maximum intensity projections (MIP) for target volume generation in 4DCT scans for lung cancer," Int. J. Radiat. Oncol., Biol., Phys. **63**, 253–260 (2005).
[35]http://www.mathworks.com/.
[36]E. E. Ahunbay, C. Peng, G. P. Chen, S. Narayanan, C. Yu, C. Lawton, and X. A. Li, "An on-line replanning scheme for interfractional variations," Med. Phys. **35**, 3607–3615 (2008).
[37]Y. Feng, C. Castro-Pareja, R. Shekhar, and C. Yu, "Direct aperture deformation: An interfraction image guidance strategy," Med. Phys. **33**, 4490–4498 (2006).
[38]Z. Gao, D. Wilkins, L. Eapen, C. Morash, Y. Wassef, and L. Gerig, "A study of prostate delineation referenced against a gold standard created from the visible human data," Radiother. Oncol. **85**, 239–246 (2007).
[39]J. D. Hoisak, K. E. Sixel, R. Tirona, P. C. Cheung, and J. P. Pignol, "Correlation of lung tumor motion with external surrogate indicators of respiration," Int. J. Radiat. Oncol., Biol. Phys. **60**, 1298–1306 (2004).
[40]D. P. Gierga, J. Brewer, G. C. Sharp, M. Betke, C. G. Willett, and G. T. Chen, "The correlation between internal and external markers for abdominal tumors: implications for respiratory gating," Int. J. Radiat. Oncol., Biol., Phys. **61**, 1551–1558 (2005).
[41]R. George, T. D. Chung, S. S. Vedam, V. Ramakrishnan, R. Mohan, E. Weiss, and P. J. Keall, "Audio-visual biofeedback for respiratory-gated radiotherapy: Impact of audio instruction and audio-visual biofeedback on respiratory-gated radiotherapy," Int. J. Radiat. Oncol., Biol., Phys. **65**, 924–933 (2006).
[42]P. R. Poulsen, B. Cho, D. Ruan, A. Sawant, and P. J. Keall, "Dynamic multileaf collimator tracking of respiratory target motion based on a single kilovoltage imager during arc radiotherapy," Int. J. Radiat. Oncol., Biol., Phys. **77**, 600–607 (2010).